

## RESEARCH ARTICLE

# Long non-coding RNAs (lncRNAs) NEAT1 and MALAT1 are differentially expressed in severe COVID-19 patients: An integrated single-cell analysis

Kai Huang<sup>1,2</sup>, Catherine Wang<sup>3</sup>, Christen Vagts<sup>1</sup>, Vanitha Raguveer<sup>3</sup>, Patricia W. Finn<sup>1,2,4\*</sup>, David L. Perkins<sup>2,5,6</sup>

**1** Division of Pulmonary, Critical Care, Sleep and Allergy, Department of Medicine, University of Illinois at Chicago, Chicago, Illinois, United States of America, **2** Department of Bioengineering, University of Illinois at Chicago, Chicago, Illinois, United States of America, **3** College of Medicine, University of Illinois at Chicago, Chicago, Illinois, United States of America, **4** Department of Microbiology and Immunology, University of Illinois at Chicago, Chicago, Illinois, United States of America, **5** Division of Nephrology, Department of Medicine, University of Illinois at Chicago, Chicago, Illinois, United States of America, **6** Department of Surgery, University of Illinois at Chicago, Chicago, Illinois, United States of America

\* [pwfinn@uic.edu](mailto:pwfinn@uic.edu)



## OPEN ACCESS

**Citation:** Huang K, Wang C, Vagts C, Raguveer V, Finn PW, Perkins DL (2022) Long non-coding RNAs (lncRNAs) NEAT1 and MALAT1 are differentially expressed in severe COVID-19 patients: An integrated single-cell analysis. *PLoS ONE* 17(1): e0261242. <https://doi.org/10.1371/journal.pone.0261242>

**Editor:** Vasu Punj, University of Southern California, UNITED STATES

**Received:** July 30, 2021

**Accepted:** November 25, 2021

**Published:** January 10, 2022

**Copyright:** © 2022 Huang et al. This is an open access article distributed under the terms of the [Creative Commons Attribution License](https://creativecommons.org/licenses/by/4.0/), which permits unrestricted use, distribution, and reproduction in any medium, provided the original author and source are credited.

**Data Availability Statement:** The raw data has been uploaded to Figshare at [https://figshare.com/projects/lncRNAs\\_NEAT1\\_and\\_MALAT1\\_in\\_COVID-19/128660](https://figshare.com/projects/lncRNAs_NEAT1_and_MALAT1_in_COVID-19/128660).

**Funding:** This work was funded by the National Heart, Lung, and Blood Institute F30HL151182 (Kai Huang), T32HL144909 (Christen Vagts), R01HL138628 (Patricia W. Finn and David L. Perkins), and the National Institute of Allergy and Infectious Diseases U01AI132898 (David L.

## Abstract

Hyperactive and damaging inflammation is a hallmark of severe rather than mild Coronavirus disease 2019 (COVID-19). To uncover key inflammatory differentiators between severe and mild COVID-19, we applied an unbiased single-cell transcriptomic analysis. We integrated two single-cell RNA-seq datasets with COVID-19 patient samples, one that sequenced bronchoalveolar lavage (BAL) cells and one that sequenced peripheral blood mononuclear cells (PBMCs). The combined cell population was then analyzed with a focus on genes associated with disease severity. The immunomodulatory long non-coding RNAs (lncRNAs) NEAT1 and MALAT1 were highly differentially expressed between mild and severe patients in multiple cell types. Within those same cell types, the concurrent detection of other severity-associated genes involved in cellular stress response and apoptosis regulation suggests that the pro-inflammatory functions of these lncRNAs may foster cell stress and damage. Thus, NEAT1 and MALAT1 are potential components of immune dysregulation in COVID-19 that may provide targets for severity related diagnostic measures or therapy.

## Introduction

The Severe Acute Respiratory Syndrome Coronavirus 2 (SARS-CoV-2) pandemic continues around the world [1, 2], but the underlying pathophysiology of coronavirus disease 2019 (COVID-19) is ill-defined. Symptoms and progression of COVID-19 vary widely [3], as some patients may be asymptomatic while others exhibit disease with varying severity [4, 5]. Common symptoms include fever, cough and fatigue that generally appear 2 to 14 days after exposure [6, 7]. Rarer symptoms include dyspnea, headache/dizziness, nausea, diarrhea and hemoptysis [8]. Severe cases of COVID-19 are distinguished by strong inflammatory responses

Perkins). The funders had no role in study design, data collection and analysis, decision to publish, or preparation of the manuscript.

**Competing interests:** The authors have declared that no competing interests exist.

that can lead to multiorgan damage and death [9]. The mechanisms that separate mild and severe disease remain poorly understood.

After viral exposure, the inflammatory response to COVID-19 commences with signaling cascades that lead to the secretion of type I interferons, cytokines and chemokines [10]. This initial exposure also activates inflammasomes, multimeric protein complexes that play an important role in triggering inflammation and the subsequent initiation of an adaptive immune response [11–13]. One such inflammasome is the Nod-like receptor pyrin domain-containing 3 (NLRP3) inflammasome, which is a major cause of cytokine storm associated with clinical manifestations of severe COVID-19 disease [14]. Coronavirus viroporin proteins can activate the NLRP3 inflammasome which subsequently regulates the secretion of IL-1 $\beta$  and IL-18 [15]. Pyroptosis, a programmed cell death pathway, that leads to immune cell depletion, is also regulated by activation of the NLRP3 inflammasome and is an important mechanism of viral pathogenesis in both SARS-CoV-2 and SARS-CoV [16–18]. These studies suggest that investigation of inflammasome regulation may elucidate understanding of COVID-19 disease pathophysiology.

Evidence is emerging that long non-coding RNAs (lncRNAs), play a substantial role in the regulation of inflammasomes as well as other inflammatory pathways [19]. Of particular interest are the lncRNAs NEAT1 and MALAT1, which have clinical relevance in multiple inflammatory disorders. NEAT1 is a potent activator of inflammasomes, particularly within macrophages [20]. Inflammatory models of several diseases including atherosclerosis, irritable bowel disease, diabetic nephropathy, and sepsis indicate that NEAT1 is a driver of inflammation and pyroptosis, identifying it as a potential target for anti-inflammatory therapy [21–24]. MALAT1 is also a potent inflammatory regulator linked to similar inflammatory disorders [25–30]. However, MALAT1 has a more nuanced inflammatory role than NEAT1 that includes immune regulatory and suppressive effects as a regulator in macrophages and T lymphocytes, as well as a source of negative feedback to the NF- $\kappa$ B pathway [31, 32]. Furthermore, both NEAT1 and MALAT1 have been recently connected to COVID-19 related inflammation, emphasizing a need for additional study of these lncRNAs [33, 34].

Single-cell studies of COVID-19 patients have found dysregulated immune compartments in the respiratory tract as well as peripheral blood [35–40]. However, it is challenging to directly compare results across studies in different tissues due to differences in cell cluster identification between physiological compartments. We postulated that simultaneous analysis of severe versus mild COVID-19 patients across respiratory and peripheral immune compartments using integrated clustering would uncover key effectors of immune dysregulation in the COVID-19 immune response. To achieve this goal, we integrated two single-cell datasets, one from bronchoalveolar lavage (BAL) and one from peripheral blood mononuclear cells (PBMCs) [35, 36], to examine disease transcriptomics across severities as well as between local and peripheral cellular environments. We utilized an unbiased analytical strategy that was agnostic to specific gene functions and focused on genes with severity-dependent expression across different cell types. Taken together, we uncovered genes contributing to the dysregulated COVID-19 immune response prominent in severe relative to mild disease. Moreover, we identified cell types where these inflammatory regulators manifest in local and peripheral compartments.

## Methods

### Dataset preprocessing and integration

We selected publicly available single-cell datasets with patient severity metrics and ample sequencing depth to pass our quality filters for integration into our combined dataset. The raw

count matrices for BAL cells and PBMCs were downloaded from the NCBI Gene Expression Omnibus (accession number GSE145926) and the COVID-19 Cell Atlas (<https://www.covid19cellatlas.org/#wilk20>), respectively. These datasets were generated from patient samples collected between January and April of 2020. Patients who were mechanically ventilated or had  $\text{PaO}_2/\text{FiO}_2 \leq 300$  mmHg indicating hypoxemia consistent with acute respiratory distress syndrome (ARDS) [41] were designated as severe patients while all others were considered to have mild disease (S1 Table). The BAL dataset contained three healthy controls while the PBMC dataset contained six (S2 Table). Both datasets were preprocessed using the R program Seurat [42]. Briefly, cells were filtered to only include cells with unique molecular identifier (UMI) counts greater than 1000, gene count between 200 and 6000, and less than 10% of genes mapping to mitochondrial genes. The function SCTransform from the Seurat package was applied to each dataset separately to regress out technical variability as well as the percentage of mitochondrial gene expression [43]. Transformed BAL and PBMC datasets were integrated with 3000 integration features and 50 integration anchors as recommended in Seurat [44]. We found that the “M3” mild patient sample from the BAL dataset contained only 369 total cells, while every other patient sample contained at least 1200 cells. The M3 sample was removed before differential expression analysis to avoid skewing results due to extremely low cell counts.

### Clustering and identification

The integrated dataset was dimension-reduced using principal component analysis (PCA) and clustered with a resolution set to 0.5 and utilizing the top 30 principle components. The clustering was visualized using uniform manifold approximation and projection (UMAP) [45]. The raw integrated dataset was normalized by applying SCTransform to the full integrated dataset. This normalized count matrix is utilized for all subsequent analysis. Marker genes for each cluster were computed using the FindAllMarkers function with the Model-based Analysis of Single-cell Transcriptomics algorithm (MAST) for differential expression with UMI count as a latent variable [46, 47]. Cluster markers were then inspected and labeled according to known cell markers [48, 49]. A second round of clustering with a resolution of 1 was then conducted to further classify subtypes of identified cells. Clusters with fewer than 300 cells were reassigned to larger clusters using Seurat integration label transfer, yielding 27 clusters at this stage. Cluster identities were then scored and verified using a signature matrix generated from flow cytometry sorted RNA-seq data of immune cells to resolve ambiguities between clusters [50]. This resulted in the merging of two natural killer cell clusters, leaving 26 total clusters. Many of these clusters consisted of similar cell types with slight differences in effector genes. Thus, clusters of the same cell type were combined in a coarse identification level with 15 clusters. The original 26 clusters were renamed as numbered subclusters of the 15 main clusters. Plots of cell clusters and key cell type markers were generated using Seurat’s plotting functions.

### Cell proportions

Cell types were tallied for each sample, and the percentage abundance of each cell type was calculated. Cell proportions for healthy controls, mild patients, and severe patients were compared using a two-sided pairwise test of equal proportion with false discovery rate (FDR) p-value adjustment. The resulting proportions were plotted using the ggplot2 R package [51].

### Differential expression

For each cell type, differentially expressed genes (DEGs) were calculated separately for BAL and PBMC cells using MAST with UMI count as a latent variable. To support MAST differential gene expression analysis between three sample groups, the Seurat built-in differential

expression function FindMarkers was modified to generate iterations of the hurdle model corresponding to each set of two compared conditions. Genes from each cell type that were differentially expressed across all three comparisons between healthy controls, mild, and severe patients were tallied. For BAL, only genes with FDR adjusted p-values less than  $1e-7$  across all comparisons were considered (17.4% of all DEGs in BAL), while PBMC DEGs were considered if all FDR adjusted p-values across comparisons for that gene were less than 0.05 (16.4% of all DEGs in PBMCs). The difference in p-value threshold was used to filter a similar proportion of genes from BAL and PBMC data due to the smaller number of DEGs detected in PBMCs (200–400 in PBMCs, 1000+ in BAL). These highly differentially expressed genes were further filtered by removing genes that were not differentially expressed across all conditions in at least 5 different cell types (1/3 of our total cell types). The lists of PBMC and BAL highly differentially expressed genes were then combined, removing duplicates.

Some of the genes identified were highly cell type specific and also had the highest residual variance with respect to the whole dataset. Since these genes represent intrinsic cell type differences rather than biologically interesting DEGs, they were removed. To determine this filter threshold, the residual variance of the top 100 variable genes were plotted in decreasing order to determine the “elbow” point where the variance stops decreasing at a rapid rate (S1 Fig). This resulted in the removal of the 21 most variable genes. We termed the 50 remaining DEGs recurrent differentially expressed genes (rDEGs) since they were found in multiple cell types and showed differential expression between patients and healthy controls as well as between severities. The rDEG expression data was exported to Monocle 3 to generate modules for gene ontology (GO) enrichment analysis. We generated 4 modules from the 50 rDEGs using the `find_gene_modules` function in Monocle 3 with 30 principle components and a resolution of 0.8 [52–54]. Differential module expression was calculated using ANOVA of aggregated module expression levels and processed with a Tukey posthoc test. Module GO enrichment was computed topGO with default settings [55]. Module and gene level plots were generated using the R packages `ggplot2`, `ComplexHeatmap`, and `Circlize` [51, 56, 57].

## Validation

We compared rDEG trends from our analysis with two additional COVID-19 datasets, one with nasopharyngeal data to compare against the local inflammatory environment of our BAL data, and one with PBMCs to compare against the peripheral environment in our PBMC data [38, 39]. Cell types from our analysis were transferred onto the validation datasets using Seurat to identify the validation cells for comparison. Each validation dataset was filtered and preprocessed separately using the same parameters as the main dataset. After preprocessing and label transfer, DEGs were generated independently for each validation set for our transferred cell types. We compared the rDEGs we focused on in the manuscript with DEG results from each validation set, noting whether the same DEG was detected and whether the direction of change was the same.

Additional step by step details for the computational methods used in this study are provided in S1 Methods and a full list of the R analysis packages and dependencies is provided in S1 File.

## Results

### Integrated PBMC and BAL analysis identified 26 clusters consolidated into 15 cell types

After quality filtering, we recovered 100,739 single cell transcriptomes. From these, we recovered 26 cell clusters from Seurat (S2 Fig). Since we identified cell types from the integrated

dataset containing both PBMCs and BAL cells, we were able to examine how each of our cell clusters behaves across both physiological compartments. The clusters did not aggregate based on sample type or patient condition (S2 Fig), indicating successful integration and clustering of the two datasets.

From the 26 clusters, 11 were identified as monocyte/macrophage (Mo/Ma) clusters. Since our clusters contain both monocytes from the PBMC sample as well as macrophages from the BAL, we designated them as MoMa clusters. Six of the MoMa clusters showed classically M1 associated transcriptomes with increased expression of VCAN, FCN1 and CD14 expression [58, 59]. These clusters also expressed other pro-inflammatory factors such as S100A8, CCL2, CCL3, CCL7, and CCL8 [60, 61]. Three other MoMa clusters showed M2 polarization with increased FN1 expression along with decreased VCAN and FCN1 expression. These M2 MoMa clusters also expressed Th2 associated inflammatory factors such as MRC1 and CCL18 [61]. All MoMa clusters expressed FCGR3A (CD16a) [58]. Two additional clusters were labeled as intermediate MoMa because they did not show distinct transcriptomes corresponding to either M1 or M2 groups. One intermediate MoMa cluster overexpressed MALAT1 while the other overexpressed metallothionein proteins including MT1F and MT1G.

We also identified two clusters of CD4+ T cells (CD4 and IL7R), one cluster of T regulatory (Treg) cells (IL2RA and LAG3) [62, 63], and three clusters of CD8+ T cells (CD8A). Two of the CD8+ T cell clusters were labeled as CD8+ memory cells due to their high CCL5 and GZMH expression [64]. Other identified immune cell clusters include natural killer (NK) cells (SPON2 and NCAM1), neutrophils (NAMPT) [50], naïve B cells (MS4A1), plasmablasts (IGJ and MZB1), plasmacytoid dendritic cells (IRF8 and PLD4) [65, 66], and myeloid dendritic cells (CD1C) and LGALS2 [50, 67]. In addition to immune cell types, we also found two epithelial clusters. One contained a mixture of epithelial and granulocyte markers including KRT19 and SLPI [50, 68] while the other also contained the additional markers PPIL6 and CFAP300 for pneumocytes and ciliary cells, respectively [69, 70].

The 26 clusters were consolidated into 15 cell types (S2 Fig) to streamline further analysis by combining clusters that are not distinguishable when examining their canonical marker expression levels. This consolidation also prevents cell groups with many clusters such as the M1 MoMa group from overshadowing those with fewer clusters in our subsequent differential gene expression ranking analysis. Cells within each cluster were compared against their original identifications from both their respective dataset, and most clusters identifications were consistent. The one exception was the intermediate MoMa type, which was predominantly composed of macrophages from BAL, but also contained a mixture of monocytes, CD4+ and CD8+ T cell identifications from PBMCs (S3 Table).

### Proinflammatory cell types are enriched in severe COVID-19 patients

Cell type proportions within BAL and PBMC sample groups showed distinct differences between patients and healthy controls as well as between mild and severe patients (Fig 1). In BAL samples of patients with severe disease, proinflammatory cells such as M1 MoMa and neutrophils showed increased abundance ( $p < .001$ , S4 Table), while immunoregulatory cell types including M2, intermediate MoMa, and Tregs were less abundant ( $p < .001$ ). BAL samples of patients with mild disease showed decreased abundance of M1 MoMa and neutrophils and increased Tregs and CD8+ memory T cells compared to healthy controls and severe patients.

In PBMCs, the trends in M1 MoMa and neutrophils are reversed. Tregs and CD8+ memory T cells are less abundant in PBMCs of mild patients. These opposing patterns may illustrate heavy recruitment of the cell types abundant in BAL, resulting in depletion in the PBMCs that

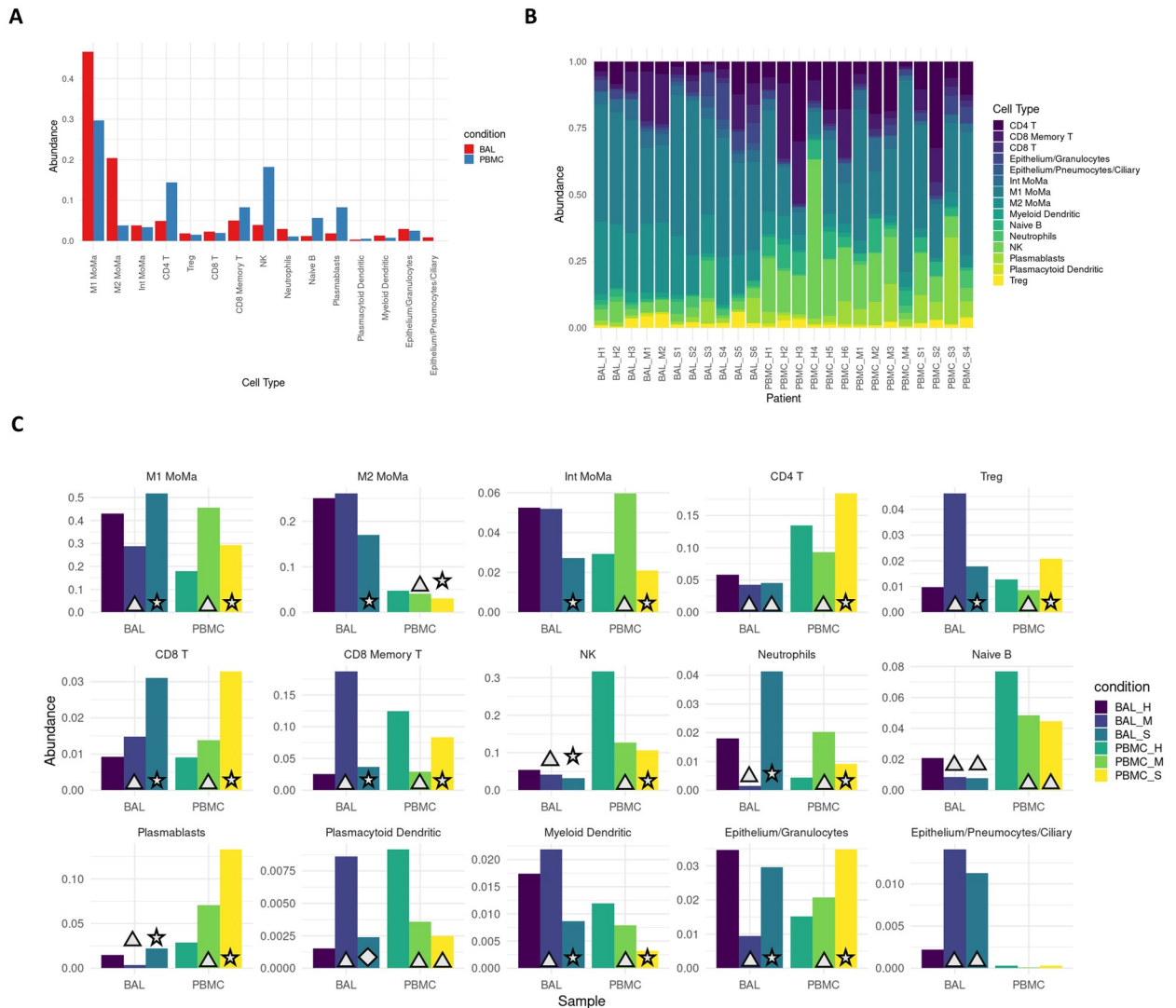


**Fig 1. Severe patients show increased proportions of proinflammatory cell types.** **A.** Overall average abundance of each major cell type for all cells. **B.** Per patient abundance of all major cell types for all cells. **C.** Per cohort (bronchoalveolar lavage (BAL) and peripheral blood mononuclear cells (PBMC)) and per condition (healthy, mild, severe) abundance for each cell type. Conditions that are significant versus their respective controls are labeled with a triangle ( $p < .05$ ). Conditions that are significant between severe and both mild as well as healthy controls are labeled with a star ( $p < .05$ ). Conditions that are significant between severe and mild, but not between severe and healthy controls, are labeled with a diamond ( $p < .05$ ). Full FDR adjusted p-value tables are reported in [S4 Table](#).

<https://doi.org/10.1371/journal.pone.0261242.g001>

results in an increase in relative abundance of non-recruited cells in PBMCs. Mild patients also showed an increase of intermediate MoMa in PBMCs, reinforcing the pattern of relative increases in abundance of immunoregulatory cell types in mild patients in both BAL and PBMC compartments.

### Recurrent DEG (rDEG) modules highlight key pathways in COVID-19 immune response

We identified an average of 1158 DEGs per cell type for BAL samples and 260 DEGs per cell type for PBMC samples ([S5](#) and [S6](#) Tables). After filtering, we identified 50 rDEGs across our

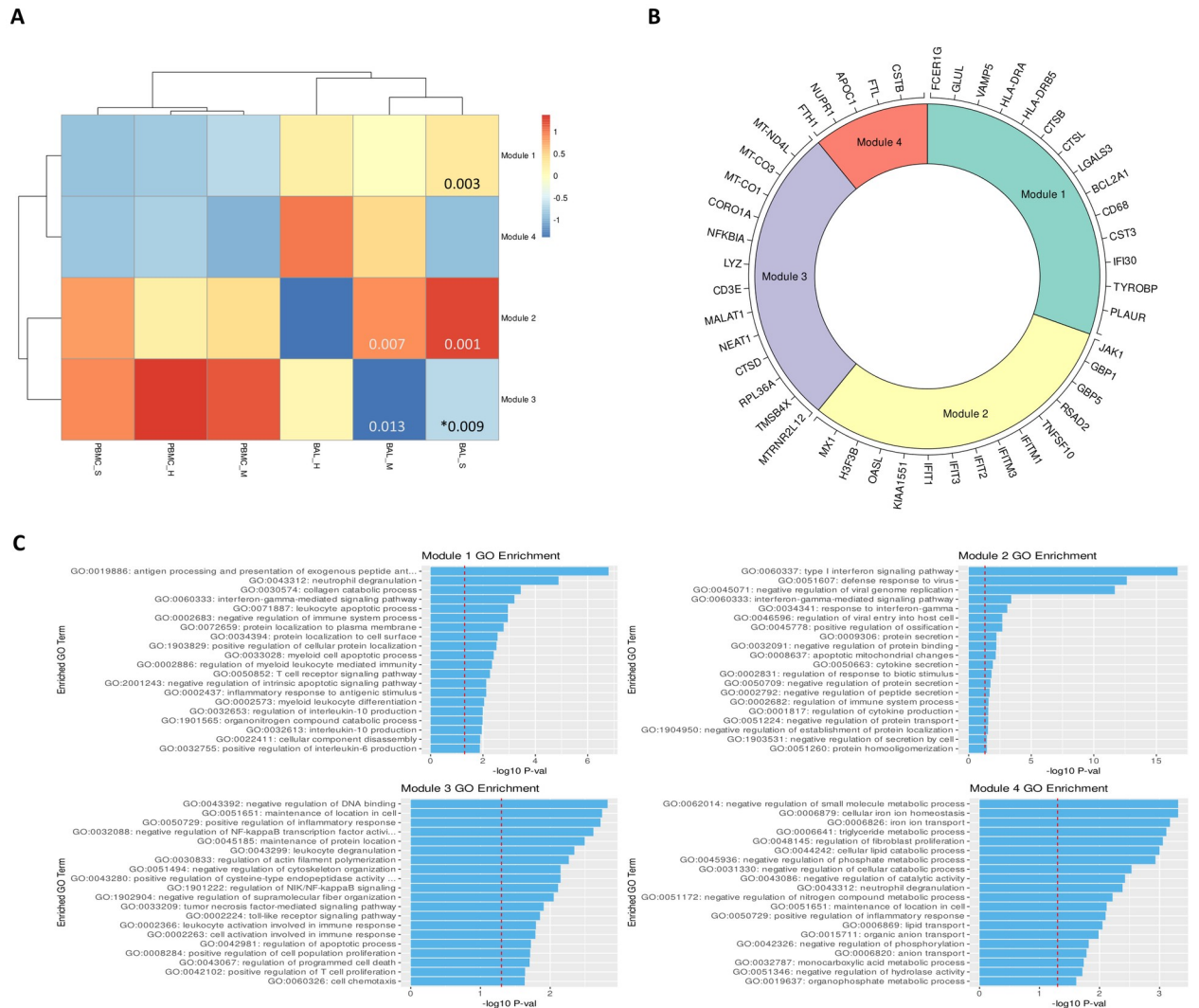


**Fig 2. rDEGs grouped into four distinct modules with immune regulation enriched GO terms.** **A.** Heatmap of modules generated from the recurrent differentially expressed genes (rDEGs). P-values are provided for comparisons with p < .05. A \* indicates comparison between severe and mild cases, while all other p-values indicate comparison with controls. **B.** Module membership for each module. Modules 1 and 4 contain a mixture of metabolic and immune response related genes. Module 2 contains genes related to interferon activated viral defense. Module 3 contains other inflammatory regulation genes and stress response genes (generated using the Circlize R package). **C.** Per module GO term enrichment showing the top enriched terms for each module and their respective p-values with the red line indicating  $-\log_{10}(0.05)$ . The first three modules contain inflammation related terms in their most enriched terms while module 4 only contains metabolism related terms.

<https://doi.org/10.1371/journal.pone.0261242.g002>

15 cell types that formed 4 distinct modules (Fig 2). Module 1 showed significant GO enrichment for developmental processes (p < .05) but did not show differential expression between conditions. Module 2 showed significance for viral defense and Type I interferon GO terms. Most genes in this module were interferon induced genes including the first three IFIT family genes, ISG15, CXCL10, and MX1. This module was significantly overexpressed in BAL of all patients versus healthy controls (p < .01).

Module 3 was enriched for macromolecule synthesis and cellular processes. This module includes the immunomodulatory lncRNAs NEAT1 and MALAT1 [20, 71]. It also includes MTRNR2L12, an anti-apoptotic lncRNA, and NFKBIA which is an NF-κB inhibitor. The module was significantly underexpressed in BAL of mild patients versus healthy controls, and

it was overexpressed in BAL of severe patients versus mild patients. Module 4 had significant terms related to negative regulation of metabolic processes. This module included the NUPR1 stress response gene as well as CSTB, which is an inhibitor of cathepsins like CTSL and CTSB that are involved in COVID-19 viral entry [72]. Module 4 was significantly underexpressed in BAL of severe patients versus healthy controls.

### **Stress response, apoptosis, and viral entry related genes show severity dependent expression**

We analyzed individual rDEGs in each of our five most abundant cell types: M1 MoMa, M2 MoMa, CD4+ T cells, NK cells, and CD8+ memory T cells (Fig 3). This analysis confirmed previous reports of downregulation of HLA genes [36, 73] such as HLA-DRA and HLA-DRB5 in COVID-19 patients, with severe patients showing the most downregulation. We also saw upregulation of interferon related genes including MX1 and IFIT1-3. This increase was greatest in mild patients, correlating with previous findings of immune exhaustion (S7 Table) [74, 75]. Further examination showed additional severity dependent patterns of differential expression of transcripts related to the stress response, cell death, and viral entry in cell types involved in the viral immune response.

The NF- $\kappa$ B inhibitor NFKBIA was upregulated in all five most abundant cell types within the BAL of severe patients compared to healthy controls and mild groups. In PBMCs of severe patients, NFKBIA was downregulated compared to healthy controls and mild patients except in CD8+ memory T cells. This pattern of localized overexpression in BAL may indicate increased NFKBIA activity in response to local hyperactivity of NF- $\kappa$ B. Furthermore, the stress response gene NUPR1, whose downregulation leads to cell death, was downregulated in M1 and M2 MoMa in the BAL of severe patients and upregulated in mild patients, indicating a pro-apoptotic shift in severe patient MoMa clusters. NUPR1 was downregulated in BAL of both mild and severe patients for NK cells, CD4+ T cells, and CD8+ memory T cells.

Mild and severe patients also had variable expression of two anti-apoptotic genes, the BCL2 inhibitor BCL2A1 and the lncRNA MTRNR2L12. BCL2A1 was significantly upregulated in BAL of severe patients over healthy controls and mild groups for M1 and M2 MoMa, NK cells, and CD4+ T cells. Mild patients showed downregulation of BCL2A1 versus healthy controls in NK and CD4+ T cells. Additionally, MTRNR2L12 was upregulated in BAL of both mild and severe patients in M1 and M2 MoMa, NK cells, CD4+ T cells and CD8+ memory T cells. The upregulation of these anti-apoptotic genes shows a defensive response to apoptotic cell stresses, particularly in BAL.

CTSL, which is a critical protein in the viral entry pathway for COVID-19, was upregulated in BAL of severe patients in M1 and M2 MoMa in mild patients and healthy controls. This suggests a faster viral entry pathway in severe patients, which may contribute to the formation of a hyperinflammatory response. In BAL of NK, CD4+ T cells, and CD8+ memory T cells, CTSL was downregulated in mild patients and upregulated in severe patients. CTSB, also implicated in viral entry, showed similar patterns.

### **NEAT1 and MALAT1 are differential regulators of inflammation in severe COVID-19**

The pro-inflammatory lncRNA NEAT1 passed our rDEG threshold in BAL samples for nine different cell types, more than any other gene in our analysis. These cell types include M1, M2 and intermediate MoMa, NK cells, CD4+ T cells, CD8+ memory T cells, naïve B cells, myeloid dendritic cells, and epithelium/basal cells (Fig 4). NEAT1 is localized to the site of infection



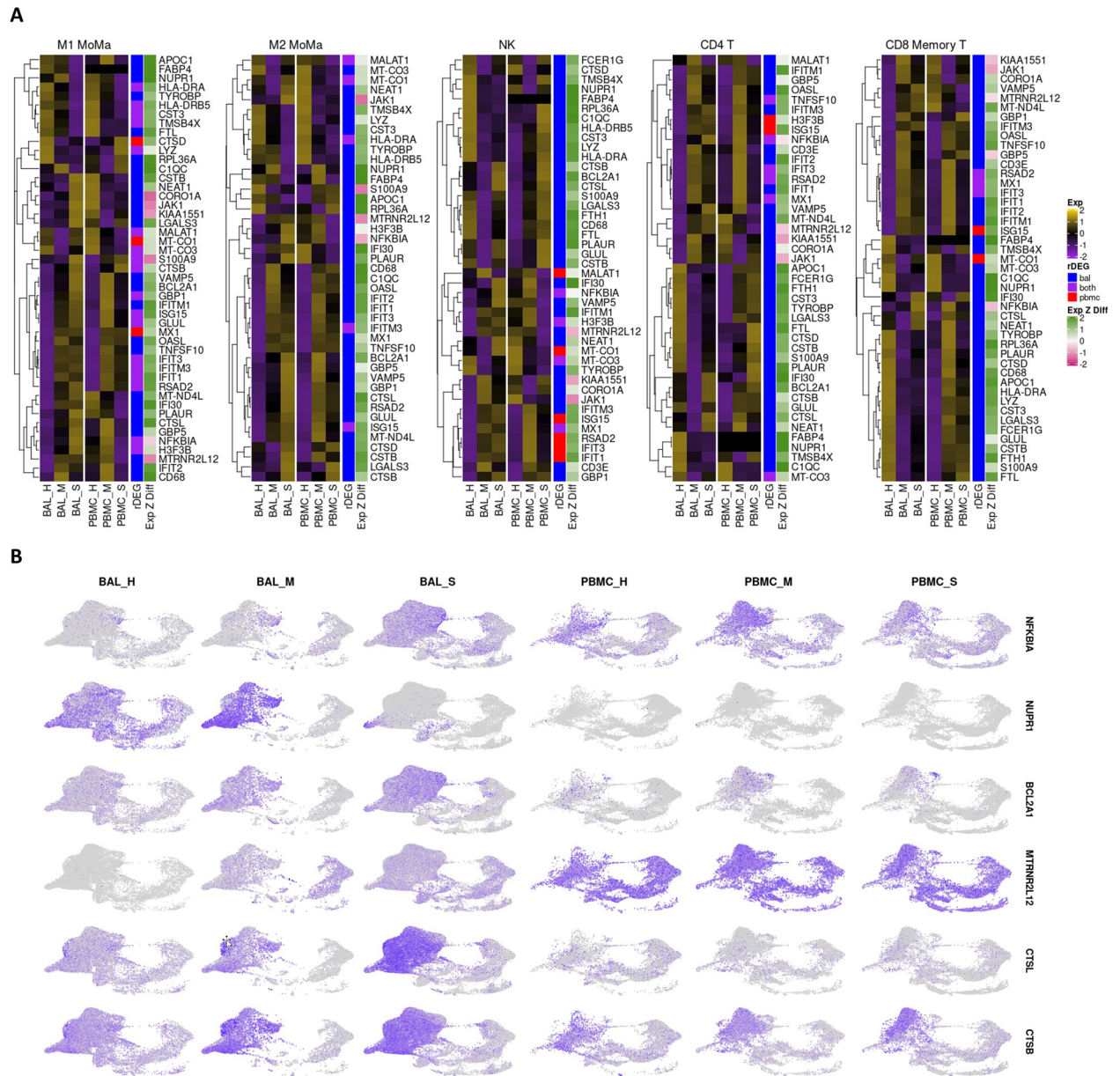


**Fig 3. rDEG expression in most abundant cell types highlights differential immune regulation between mild and severe patients in both BAL and PBMC cohorts.** **A.** Heatmaps visualizing rDEGs within each of the top five most abundant cell types in our dataset (generated using the ComplexHeatmap R package). For each cell type, the full rDEG list was filtered via the same p-values ( $p < 10e-7$  for BAL,  $p < .05$  for PBMC) and only rDEGs that are differentially expressed below these thresholds for either BAL or PBMC are included in the plot. Expression levels are normalized separately for each cohort. The first sidebar indicates which cohort the particular gene passed the rDEG threshold for, while the second sidebar indicates the ratio of expression of the particular gene between BAL and PBMC with green (positive values) indicating higher expression levels detected in BAL. Full p-value tables are provided in *S7 Table*. **B.** Visualization of select rDEGs representing pathways outside of the main interferon activated gene group that are relevant to disease. These genes are visualized separately for each cohort and condition using the sample UMAP projection of cell types from *Fig 1*. Each gene shows cell type, cohort, and condition specific differences in localization across the dataset.

<https://doi.org/10.1371/journal.pone.0261242.g003>

and inflammation since it is not differentially expressed in PBMCs. Additionally, among rDEGs, it has one of the highest averages in log2-fold change between severe and mild patients (*Fig 4*). NEAT1 is overexpressed in BAL of severe patients and underexpressed in mild patients. The epithelial/basal cell group is the exception where mild groups also show NEAT1

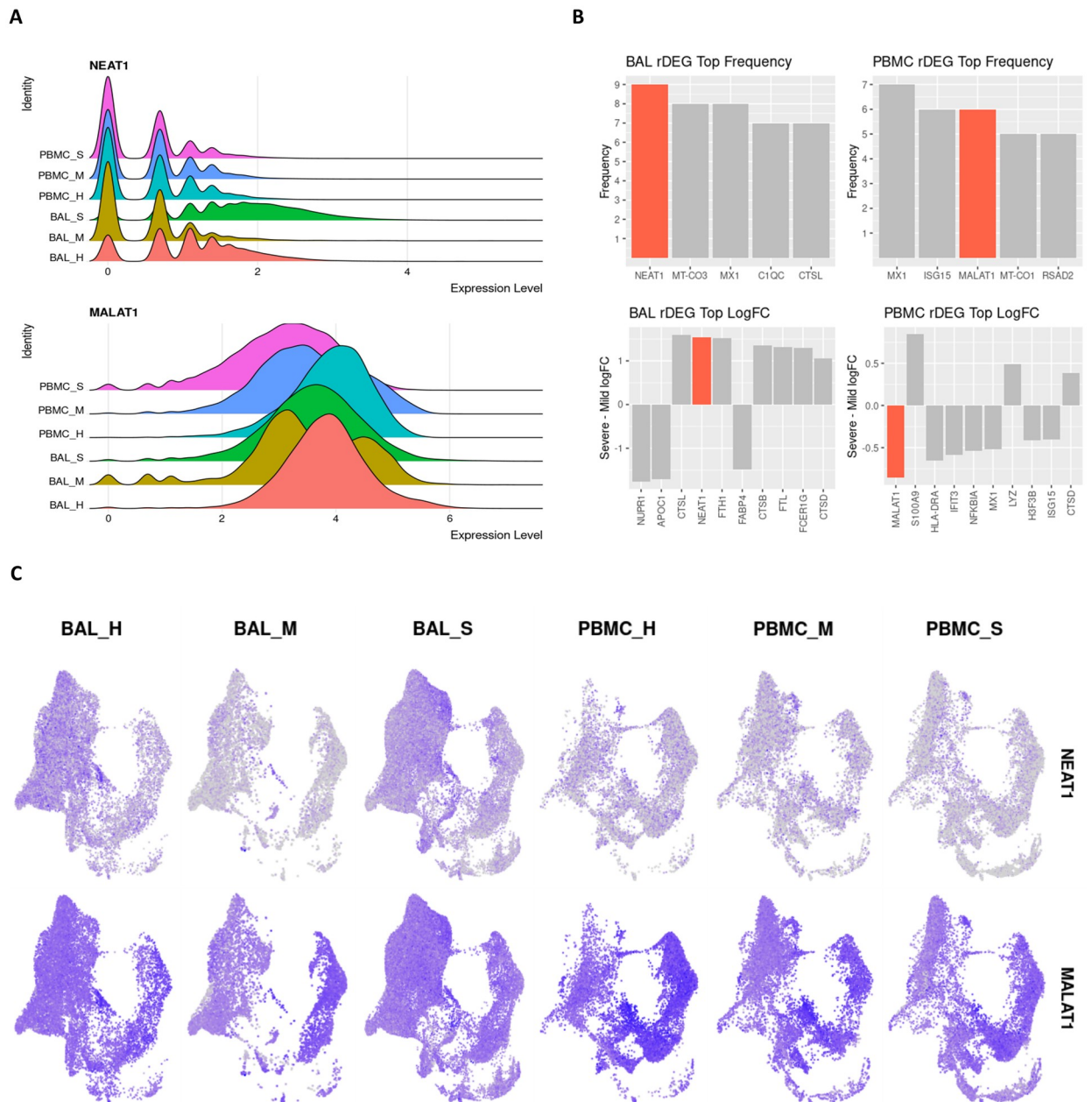


**Fig 4. lncRNAs NEAT1 and MALAT1 are strongly differentially expressed between severe and mild patients and represent key inflammatory regulators in BAL and PBMC respectively.** A. Violin plots showing overall expression level density across patient conditions in the entire dataset. Even at the full dataset scale, these distributions show that NEAT1 is overexpressed in BAL of severe patients while MALAT1 is underexpressed in PBMCs of severe patients. B. Frequency of detection across cell types for rDEGs shows NEAT1 as the most detected rDEG in BAL, with MALAT1 tied for second among rDEGs in PBMC. The top log<sub>2</sub>-fold change of rDEGs in severe versus mild patients also shows NEAT1 and MALAT1 among the rDEGs with the highest absolute change between severe and mild conditions. C. Visualization of NEAT1 and MALAT1 via UMAP projection shows more cell type localized expression in NEAT1. It is also clearly underexpressed in mild BAL cases. MALAT1 also shows a more subtle but significant underexpression in severe patient PBMCs.

<https://doi.org/10.1371/journal.pone.0261242.g004>

overexpression over healthy controls, but expression is still significantly higher in severe patients versus mild patients.

Another immunomodulatory lncRNA, MALAT1, was the second most frequent rDEG in PBMCs. It passed our rDEG threshold in 6 cell types (tied with ISG15) and 3 cell types in BAL.

In BAL derived M1 and M2 MoMa, MALAT1 was underexpressed in mild patients compared to both healthy controls and severe patients. In CD4+ T cells, MALAT1 shows consistent overexpression in mild patients and underexpression in severe patients. In PBMCs, MALAT1 was underexpressed in severe patients versus both healthy controls and mild patients in M1, M2 and intermediate MoMa, NK cells, plasmablasts, and epithelial/basal cells.

### Validation of rDEG expression patterns

We projected the cell type classifications in our analysis via Seurat's label transfer feature to two other COVID-19 datasets, one with nasopharyngeal samples [38] and one with PBMC samples [39]. Comparison of cell labels from the original datasets versus our transferred labels shows general agreement among the cell IDs, allowing us to use our cell type labels for direct comparison of rDEG patterns in the validation data (S3 and S4 Figs). We compared rDEG expression patterns of the genes analyzed in the previous two sections in the same five cell types. Among each gene's statistically significant changes in our analysis between healthy, mild, and severe cases, 36.3% were significant in our validation cohorts. However, more than two thirds of the non-significant findings in validation were from comparisons with healthy control in the nasopharyngeal dataset. This is likely due to the small number of cells recovered from these controls after filtering. Only 1148 cells were recovered from control samples after filtering compared to 35,715 and 25,546 for moderate and severe cases respectively. Among the findings that were significant in both our data and in validation, we found that 79% were significant in the same direction. Notably, NEAT1 showed 100% agreement in validation of BAL while MALAT1 showed 100% agreement in validation of PBMCs (S8–S10 Tables).

### Discussion

Our analysis of BAL and PBMC single-cell data in COVID-19 patients has elucidated key differences between mild and severe disease. We were able to combine cells from both PBMC and BAL in an integrated analysis. Although our intermediate MoMa group had a mixed group of cells, our overall identifications were consistent across both datasets. Furthermore, the cells in the intermediate MoMa group consisted of cells with weak expression of a wide range of canonical markers. These cells may be intermediate immune cells from different lineages that share a similar transcriptomic profile. By conducting analysis simultaneously on cells from the local infection site as well as the peripheral immune system, we contrast how the disease manifests and interacts across both compartments. We have identified differentially expressed genes that vary with severity, are highly differentially expressed across multiple cell types, and represent key functions related to the hyperinflammatory disease state.

NEAT1 was the most widely differentially expressed gene across cell types within BAL; it also exhibited a high log-fold change that correlated with disease severity. The ubiquity of NEAT1, its specific localization to BAL cells, and its pro-inflammatory functions suggests that it may be a key mediator of the inflammation seen in severe COVID-19. NEAT1 is a well characterized activator of the NLRP3 inflammasome, as well as the NLRC4 and AIM2 inflammasomes, which in turn amplify the inflammatory response [20]. However, an overactive immune response contributes to lasting tissue damage in severe COVID-19 disease. Intense inflammation through activation of the NLRP3 inflammasome can also lead to pyroptosis, driven by the upregulation of NEAT1 [20, 21]. These highly inflammatory and damaging effects of NEAT1 illustrate how overexpression in severe patients might lead to the inflammatory tissue damage seen in severe COVID-19.

MALAT1 also exerts various immunological effects including the mediation of NLRP3 inflammasome activation [19, 76]. MALAT1 has been linked to M1-like activity in

macrophages, promoting inflammation [77]. Our finding that MALAT1 is overexpressed in BAL MoMa of severe versus mild patients suggests that it might be involved in precipitating a shift towards M1 macrophages that exacerbates inflammation. This is further supported by our findings that severe patients show expansion of M1 macrophages and decrease of M2 and intermediate macrophages in BAL, while mild patients show decrease of M1 macrophages. Furthermore, MALAT1 was overexpressed in CD4+ T cells of mild patients. This is also reflective of MALAT1's protective role in T cells. Loss of MALAT1 expression has been shown to push T cells towards the inflammatory Th1 and Th17 phenotypes while also decreasing Treg differentiation [31]. This function matches our observed increase in abundance of Tregs in mild patients. Thus, the upregulation of MALAT1 in mild patients may be contributing to the more subdued immune response observed in these patients.

The severity dependent differential expression of other genes in our analysis provides further evidence of increased cellular stress reflective of a NEAT1 and MALAT1 enhanced hyper-inflammatory state. NF- $\kappa$ B is induced in COVID-19 infection [78]. Although we did not detect differential activity of NF- $\kappa$ B directly, we found upregulation of its inhibitor NFKBIA in BAL of severe patients which suggests a feedback response to strong NF- $\kappa$ B activity. NFKBIA's downregulation in PBMCs of severe patients may be due to localization of cells expressing NFKBIA to the site of infection in attempts to regulate the hyperactive inflammatory state [79]. The upregulation of BCL2A1 and MTRNR2L12 is also indicative of extensive cellular stress [80, 81]. While MTRNR2L12 is upregulated in both mild and severe disease, BCL2A1 is upregulated exclusively in severe disease. The increased activity of these anti-apoptotic genes, particularly in BAL of severe patients, shows additional evidence of the cellular stress induced by infection and inflammation. These genes may be responding to pyroptosis pathways triggered by inflammasome activation via NEAT1 and MALAT1. Further evidence of inflammatory cell damage is seen in the downregulation of NUPR1 in BAL of M1 and M2 macrophages of severe patients with upregulation in mild patients. Downregulation of this stress response gene has been shown to cause mitochondrial dysfunction and ROS production that can lead to cell death [82]. Lastly, our observation that CTSL, a protein crucial for COVID-19 viral entry is upregulated across multiple cell types in severe patients provides a potential initial mechanism for the induction of the NEAT1 and MALAT1 mediated inflammatory state through increased efficiency of viral entry [72]. Recently, additional independent evidence and reviews have emerged highlighting expression of NEAT1 and MALAT1 in both *in vitro* and *in vivo* samples of COVID-19 infection [83–86]. These additional studies provide further evidence that the patterns of lncRNA expression presented in this study are highly associated with COVID-19 related inflammation.

Our study presents the first report of lncRNA associations in an integrated single-cell analysis of patient tissues in COVID-19 infection. By leveraging dataset integration to create a set of consistent cell identifications between BAL and PBMC environments, we provide a global view of lncRNA involvement in COVID-19 with specific insights with respect to cell-type, immunological compartment, and disease severity. We also created a unique rDEG approach which aided in simplifying a *de novo* exploration of fifteen cell types across three subject groups and two immunological compartments. Our novel single-cell level lncRNA findings provides granular details that will enable additional targeted studies.

Limitations in our study include the small sample size, variable clinical presentation and differing treatments. Additionally, time from presentation to sample collection varied across patients. The stratification of patients as severe or mild may also introduce unknown factors due to patient variability in presentation and classification. Although our validation shows promising reproduction of expression patterns, additional studies with more subjects and stringent recruiting and sample collection would further elucidate these findings.

Furthermore, the datasets we analyzed were generated from patient samples collected between January and April 2020, before the first SARS-CoV-2 variants were designated by the World Health Organization. While the overall trends in our data are reflected in recent work on lncRNAs in COVID-19, there remains a lack of variant specific studies [85]. Additional work on the expression of lncRNAs in variant specific samples may uncover further insights.

We have demonstrated a clear ensemble of differential gene activity associated with severe disease in COVID-19 infection that revolves around the lncRNAs NEAT1 and MALAT1. Their specific activity changes in severe patients, coupled with inflammasome promoting functions, suggest important roles in the COVID-19 hyperinflammatory process. These findings indicate that NEAT1 and MALAT1 may be candidates for treatment targeting or biological marker exploration.

## Supporting information

**S1 Fig. Filtering of genes with extremely high residual variance.** A. A plot of mean expression levels versus residual variance for all genes detected in dataset. Genes with the highest residual variance are nearly all immunoglobulin and ribosome genes. B. Plot of 100 genes with highest residual variance in descending order. The rate of variance decrease stabilizes after the 21<sup>st</sup> gene. C. Table of top 21 genes filtered out of downstream analysis due to very high residual variance.

(BMP)

**S2 Fig. Unbiased clustering of combined BAL and PBMC data reveals common cell types between cohorts and sample conditions.** A/B. Uniform manifold approximation and projection (UMAP) plots showing the distribution of all cells in both cohorts within defined cell types. Plot A shows the 15 major cell groups we identified with labels over the cluster centers. Plot B shows the subclusters making up those groups. The major groups are abbreviated as prefixes with a letter suffix indicating subgroup. M1, M2 and Int are the macrophage/monocytes. NK is natural killer cells, E/G is epithelial cells and granulocytes, and E/P/C is epithelia, pneumocyte, and ciliary cells. C. Select markers for major cell groups plotted on the same UMAP projection. This illustrates the specificity of these markers for different regions of the plot corresponding to our respective cell types. D. Dot plot visualization of top markers utilized for identification of each cell cluster. The size of each dot indicates the percentage of cells with detectable expression of each gene, with color indicating expression level. E. Splitting the UMAP by cohort and by severity, with “H” indicating healthy control, “M” indicating mild disease, and “S” indicating severe disease illustrates that cell clusters do not organize according to sample type or patient condition, indicating successful integration of the datasets.

(BMP)

**S3 Fig. Transferred cell identities correspond to original cell identities from the nasopharyngeal validation set.** Dot plot shows cells from the nasopharyngeal validation dataset, identified by their transferred labels on the Y axis and their original labels on the X axis. Color of each dot indicates the numeric log frequency of cells that fit each corresponding set of labels. The size of each dot represents the percentage of each transferred cell types which is represented by each original cell type. From left to right, the full cell type names from the nasopharyngeal dataset are: non-resident macrophage (nrMa), monocyte-derived macrophage (MoD-Ma), monocyte-derived dendritic cell (moDC), resident macrophage (rMa), cytotoxic T cell (CTL), regulatory T cell (Treg), natural killer T cell (NKT), proliferating natural killer T cell (NKT-p), natural killer cells (NK), neutrophils (Neu), B cells, plasmacytoid dendritic cell (pDC), basal cell, ciliated cell, differentiating ciliated cell, FOXP3+ epithelial cell, ionocyte,

interferon responsive cell (IRC), mast cell (MC), epithelial outliers, secretory, differentiating secretory, squamous, and unknown epithelial.  
(BMP)

**S4 Fig. Transferred cell identities correspond to original cell identities from the PBMC validation set.** Dot plot shows cells from the PBMC validation set, identified by their transferred labels on the Y axis and their original labels on the X axis. Color of each dot indicates the numeric log frequency of cells that fit each corresponding set of labels. The size of each dot represents the percentage of each transferred cell type represented by each original cell type. This dataset contained several cell types where the same label was applied to more than one subcluster, resulting in numeric suffixes for similar cell types. mDCs correspond to myeloid dendritic cells and pDCs correspond to plasmacytoid dendritic cells.  
(BMP)

**S1 Table. Key characteristics of patients within each dataset.** Patient information from the BAL and PBMC cohorts used in this analysis. Patients who were intubated or had  $\text{PaO}_2/\text{FiO}_2 \leq 300$  mmHg were classified as severe. In BAL, patient “Mild 3” had only 369 cells recovered after filtering and was only used for initial clustering. Exact ages were not available in the PBMC cohort. The first patient in this cohort was sampled twice, once while classified as a mild patient, and once after their symptoms worsened and required mechanical ventilation. Several patients in the PBMC cohort received azithromycin, which can have immunomodulatory effects before sample collection.  
(PDF)

**S2 Table. Demographic characteristics of healthy subjects.** All healthy controls used from both the BAL and PBMC cohorts are listed.  
(PDF)

**S3 Table. Cell identities from original datasets versus new combined identification.** For BAL and PBMCs, each cell’s original cell identification and new identification are tabulated for the 26 clusters in the subgroup sheets, and the 15 consolidated cell groups in the coarse sheets.  
(XLSX)

**S4 Table. P-value tables for cell proportion comparisons across each cell type.** Conditions compared are listed in the first two columns, and FDR adjusted p-values are listed in the third column. Each sheet is labeled by cell type.  
(XLSX)

**S5 Table. DEGs for BAL and PBMC samples respectively, separated by cell type, with raw p-values as well as FDR adjusted p-values.** Each sheet is labeled by cell type. Column headings include indicators for which conditions are being compared where applicable. The conditions are numbered: “1 = healthy control”, “2 = mild COVID-19 patient”, “3 = severe COVID-19 patient”. For example, the prefix “g2\_1” indicates the comparison of mild patient expression levels minus healthy control expression levels. Log-fold change is reported relative to the natural log. Columns labeled “pct.1”, “pct.2”, or “pct.3” indicate the percentage of cells in the condition corresponding to that number with detectable expression of a particular gene.  
(XLSX)

**S6 Table. DEGs for BAL and PBMC samples respectively, separated by cell type, with raw p-values as well as FDR adjusted p-values.** Each sheet is labeled by cell type. Column headings include indicators for which conditions are being compared where applicable. The

conditions are numbered: “1 = healthy control”, “2 = mild COVID-19 patient”, “3 = severe COVID-19 patient”. For example, the prefix “g2\_1” indicates the comparison of mild patient expression levels minus healthy control expression levels. Log-fold change is reported relative to the natural log. Columns labeled “pct.1”, “pct.2”, or “pct.3” indicate the percentage of cells in the condition corresponding to that number with detectable expression of a particular gene.

(XLSX)

**S7 Table. rDEGs with their expression levels in each cell type where each rDEG’s adjusted p-values passed the p-value filter as defined in our methods section.** Column headings include indicators for which conditions are being compared where applicable. The conditions are numbered: “1 = healthy control”, “2 = mild COVID-19 patient”, “3 = severe COVID-19 patient”. For example, the prefix “g2\_1” indicates the comparison of mild patient expression levels minus healthy control expression levels. Log-fold change is reported relative to the natural log. Columns labeled “pct.1”, “pct.2”, or “pct.3” indicate the percentage of cells in the condition corresponding to that number with detectable expression of a particular gene. The “celltype” and “sample” columns indicate which cell type and which sample condition the rDEG passed filter in.

(XLSX)

**S8 Table. Comparisons between rDEGs discussed in our results shows strong agreement in validation datasets. A/B.** Tables representing the tally of differential expression results of our discussed rDEGs which agreed or disagreed between analysis and validation groups based on the direction of detected differential expression. Tables are split by BAL/nasopharyngeal and PBMC groups. The first three columns correspond to cases where a comparison is not available due to a lack of differential expression detected in the original analysis (na.orig), the validation set (na.val), or both (na.all). The top half of each table reports the results for severe versus mild cases only (SvsM) while the bottom half reports results for all three comparisons: healthy versus mild, healthy versus severe, and severe versus mild.

(PDF)

**S9 Table. Per gene level validation tables for BAL and PBMC groups respectively.** Each sheet name corresponds to the cell type presented. Row names indicate the gene being compared, and column names indicate the cohorts being compared: healthy (H), mild COVID (M), and severe COVID (S). When differential expression is detected in both the original analysis and validation, the column is labeled “agree” if the change occurred in the same direction and “disagree” if it is opposite. Other labels indicate where a comparison is not available due to a lack of differential expression detected in the original analysis (na.orig), the validation set (na.val), or both (na.all).

(XLSX)

**S10 Table. Per gene level validation tables for BAL and PBMC groups respectively.** Each sheet name corresponds to the cell type presented. Row names indicate the gene being compared, and column names indicate the cohorts being compared: healthy (H), mild COVID (M), and severe COVID (S). When differential expression is detected in both the original analysis and validation, the column is labeled “agree” if the change occurred in the same direction and “disagree” if it is opposite. Other labels indicate where a comparison is not available due to a lack of differential expression detected in the original analysis (na.orig), the validation set (na.val), or both (na.all).

(XLSX)

**S1 File. Output of the sessionInfo() function in R showing packages loaded for this analysis along with all dependencies and operating system details.**

(TXT)

**S1 Methods. Detailed computational methods.**

(DOCX)

## Author Contributions

**Conceptualization:** Kai Huang.

**Funding acquisition:** Kai Huang, Patricia W. Finn, David L. Perkins.

**Investigation:** Kai Huang, Catherine Wang, Vanitha Raguveer.

**Methodology:** Kai Huang.

**Software:** Kai Huang.

**Supervision:** Christen Vagts, Patricia W. Finn, David L. Perkins.

**Visualization:** Kai Huang.

**Writing – original draft:** Kai Huang, Catherine Wang.

**Writing – review & editing:** Kai Huang, Catherine Wang, Christen Vagts, Vanitha Raguveer, Patricia W. Finn, David L. Perkins.

## References

1. Sanche S, Lin YT, Xu C, Romero-Severson E, Hengartner N, Ke R. RESEARCH High Contagiousness and Rapid Spread of Severe Acute Respiratory Syndrome Coronavirus 2. *Emerg Infect Dis.* 2020; 26: 1470–1477. <https://doi.org/10.3201/eid2607.200282> PMID: 32255761
2. Li R, Pei S, Chen B, Song Y, Zhang T, Yang W, et al. Substantial undocumented infection facilitates the rapid dissemination of novel coronavirus (SARS-CoV-2). *Science (80-).* 2020; 368: 489–493. <https://doi.org/10.1126/science.abb3221> PMID: 32179701
3. García LF. Immune Response, Inflammation, and the Clinical Spectrum of COVID-19. *Frontiers in Immunology.* Frontiers Media S.A.; 2020. <https://doi.org/10.3389/fimmu.2020.01441> PMID: 32612615
4. Vetter P, Eckerle I, Kaiser L. Covid-19: A puzzle with many missing pieces. *The BMJ.* BMJ Publishing Group; 2020. <https://doi.org/10.1136/bmj.m627> PMID: 32075791
5. Wang F, Qu M, Zhou X, Zhao K, Lai C, Tang Q, et al. The timeline and risk factors of clinical progression of COVID-19 in Shenzhen, China. *J Transl Med.* 2020; 18: 270. <https://doi.org/10.1186/s12967-020-02423-8> PMID: 32620125
6. Guan W, Ni Z, Hu Y, Liang W, Ou C, He J, et al. Clinical Characteristics of Coronavirus Disease 2019 in China. *N Engl J Med.* 2020; 382: 1708–1720. <https://doi.org/10.1056/NEJMoa2002032> PMID: 32109013
7. Goyal P, Choi JJ, Pinheiro LC, Schenck EJ, Chen R, Jabri A, et al. Clinical Characteristics of Covid-19 in New York City. *N Engl J Med.* 2020; 382: 2372–2374. <https://doi.org/10.1056/NEJMc2010419> PMID: 32302078
8. Tay MZ, Poh CM, Rénia L, MacAry PA, Ng LFP. The trinity of COVID-19: immunity, inflammation and intervention. *Nature Reviews Immunology.* Nature Research; 2020. pp. 363–374. <https://doi.org/10.1038/s41577-020-0311-8> PMID: 32346093
9. Zaim S, Chong JH, Sankaranarayanan V, Harky A. COVID-19 and Multiorgan Response. *Current Problems in Cardiology.* Mosby Inc.; 2020. <https://doi.org/10.1016/j.cpcardiol.2020.100618> PMID: 32439197
10. van den Berg DF, te Velde AA. Severe COVID-19: NLRP3 Inflammasome Dysregulated. *Front Immunol.* 2020; 11: 1580. <https://doi.org/10.3389/fimmu.2020.01580> PMID: 32670297
11. Evavold CL, Kagan JC. How Inflammasomes Inform Adaptive Immunity. *Journal of Molecular Biology.* Academic Press; 2018. pp. 217–237. <https://doi.org/10.1016/j.jmb.2017.09.019> PMID: 28987733



12. Li G, Fan Y, Lai Y, Han T, Li Z, Zhou P, et al. Coronavirus infections and immune responses. *Journal of Medical Virology*. John Wiley and Sons Inc.; 2020. pp. 424–432. <https://doi.org/10.1002/jmv.25685> PMID: 31981224
13. Guo H, Callaway JB, Ting JPY. Inflammasomes: Mechanism of action, role in disease, and therapeutics. *Nature Medicine*. Nature Publishing Group; 2015. pp. 677–687. <https://doi.org/10.1038/nm.3893> PMID: 26121197
14. Freeman TL, Swartz TH. Targeting the NLRP3 Inflammasome in Severe COVID-19. *Frontiers in Immunology*. Frontiers Media S.A.; 2020. p. 1518. <https://doi.org/10.3389/fimmu.2020.01518> PMID: 32655582
15. Farag NS, Breiting U, Breiting HG, El Azizi MA. Viroporins and inflammasomes: A key to understand virus-induced inflammation. *International Journal of Biochemistry and Cell Biology*. Elsevier Ltd; 2020. p. 105738. <https://doi.org/10.1016/j.biocel.2020.105738> PMID: 32156572
16. Yap JKY, Moriyama M, Iwasaki A. Inflammasomes and Pyroptosis as Therapeutic Targets for COVID-19. *J Immunol*. 2020; 205: 307–312. <https://doi.org/10.4049/jimmunol.2000513> PMID: 32493814
17. Yue Y, Nabar NR, Shi CS, Kamenyeva O, Xiao X, Hwang IY, et al. SARS-Coronavirus Open Reading Frame-3a drives multimodal necrotic cell death. *Cell Death Dis*. 2018; 9: 1–15.
18. Bergsbaken T, Fink SL, Cookson BT. Pyroptosis: Host cell death and inflammation. *Nature Reviews Microbiology*. NIH Public Access; 2009. pp. 99–109. <https://doi.org/10.1038/nrmicro2070> PMID: 19148178
19. Menon MP, Hua K-FF. The Long Non-coding RNAs: Paramount Regulators of the NLRP3 Inflammasome. *Frontiers in Immunology* Sep 25, 2020 p. 569524. <https://doi.org/10.3389/fimmu.2020.569524> PMID: 33101288
20. Zhang P, Cao L, Zhou R, Yang X, Wu M. The lncRNA Neat1 promotes activation of inflammasomes in macrophages. *Nat Commun*. 2019; 10: 1–17.
21. Zhan J-F, Huang H-W, Huang C, Hu L-L, Xu W-W. Long Non-Coding RNA NEAT1 Regulates Pyroptosis in Diabetic Nephropathy via Mediating the miR-34c/NLRP3 Axis. *Kidney Blood Press Res*. 2020; 45: 589–602. <https://doi.org/10.1159/000508372> PMID: 32721950
22. Liu R, Tang A, Wang X, Chen X, Zhao L, Xiao Z, et al. Inhibition of lncRNA NEAT1 suppresses the inflammatory response in IBD by modulating the intestinal epithelial barrier and by exosome-mediated polarization of macrophages. *Int J Mol Med*. 2018; 42: 2903–2913. <https://doi.org/10.3892/ijmm.2018.3829> PMID: 30132508
23. Wang L, Xia JW, Ke ZP, Zhang BH. Blockade of NEAT1 represses inflammation response and lipid uptake via modulating miR-342-3p in human macrophages THP-1 cells. *J Cell Physiol*. 2019; 234: 5319–5326. <https://doi.org/10.1002/jcp.27340> PMID: 30259979
24. Li Y, Guo W, Cai Y. NEAT1 promotes LPS-induced inflammatory injury in macrophages by regulating miR-17-5p/TLR4. *Open Med*. 2020; 15: 38–49. <https://doi.org/10.1515/med-2020-0007> PMID: 32099901
25. Zhou Q, Run Q, Li C-Y, Xiong X-Y, Wu X-L. lncRNA MALAT1 Promotes STAT3-Mediated Endothelial Inflammation by Counteracting the Function of miR-590. *Cytogenet Genome Res*. 2020; 160: 565–578. <https://doi.org/10.1159/000509811> PMID: 33022677
26. Wang L, Liu J, Xie W, Li G, Yao L, Zhang R, et al. Overexpression of MALAT1 relates to lung injury through sponging miR-425 and promoting cell apoptosis during ARDS. *Can Respir J*. 2019; 2019. <https://doi.org/10.1155/2019/1871394> PMID: 31871512
27. Biswas S, Thomas AA, Chen S, Aref-Eshghi E, Feng B, Gonder J, et al. MALAT1: An Epigenetic Regulator of Inflammation in Diabetic Retinopathy. *Sci Rep*. 2018; 8: 1–15.
28. Wei S, Liu Q. Long noncoding RNA MALAT1 modulates sepsis-induced cardiac inflammation through the miR-150-5p/NF- $\kappa$ B axis. *Int J Clin Exp Pathol*. 2019; 12: 3311–3319. Available: <http://www.ncbi.nlm.nih.gov/pubmed/31934174>
29. Wei L, Li J, Han Z, Chen Z, Zhang Q. Silencing of lncRNA MALAT1 Prevents Inflammatory Injury after Lung Transplant Ischemia-Reperfusion by Downregulation of IL-8 via p300. *Mol Ther—Nucleic Acids*. 2019; 18: 285–297. <https://doi.org/10.1016/j.omtn.2019.05.009> PMID: 31604167
30. Cai LJ, Tu L, Huang XM, Huang J, Qiu N, Xie GH, et al. lncRNA MALAT1 facilitates inflammasome activation via epigenetic suppression of Nrf2 in Parkinson's disease. *Mol Brain*. 2020; 13: 130. <https://doi.org/10.1186/s13041-020-00656-8> PMID: 32972446
31. Masoumi F, Ghorbani S, Talebi F, Branton WG, Rajaei S, Power C, et al. Malat1 long noncoding RNA regulates inflammation and leukocyte differentiation in experimental autoimmune encephalomyelitis. *J Neuroimmunol*. 2019; 328: 50–59. <https://doi.org/10.1016/j.jneuroim.2018.11.013> PMID: 30583215
32. Zhao G, Su Z, Song D, Mao Y, Mao X. The long noncoding RNA MALAT1 regulates the lipopolysaccharide-induced inflammatory response through its interaction with NF- $\kappa$ B. *FEBS Lett*. 2016; 590: 2884–2895. <https://doi.org/10.1002/1873-3468.12315> PMID: 27434861

33. Meydan C, Madrer N, Soreq H. The Neat Dance of COVID-19: NEAT1, DANCR, and Co-Modulated Cholinergic RNAs Link to Inflammation. *Front Immunol.* 2020; 11: 2638. <https://doi.org/10.3389/fimmu.2020.590870> PMID: 33163005
34. Tang H, Gao Y, Li Z, Miao Y, Huang Z, Liu X, et al. The noncoding and coding transcriptional landscape of the peripheral immune response in patients with COVID-19. *Clin Transl Med.* 2020; 10: e200. <https://doi.org/10.1002/ctm2.200> PMID: 33135345
35. Liao M, Liu Y, Yuan J, Wen Y, Xu G, Zhao J, et al. Single-cell landscape of bronchoalveolar immune cells in patients with COVID-19. *Nat Med.* 2020; 1–3.
36. Wilk AJ, Rustagi A, Zhao NQ. A single-cell atlas of the peripheral immune response in patients with severe COVID-19. *Nat Med.* 2020. <https://doi.org/10.1038/s41591-020-0944-y> PMID: 32514174
37. Zhang JY, Wang XM, Xing X, Xu Z, Zhang C, Song JW, et al. Single-cell landscape of immunological responses in patients with COVID-19. *Nat Immunol.* 2020; 21: 1107–1118. <https://doi.org/10.1038/s41590-020-0762-x> PMID: 32788748
38. Chua RL, Lukassen S, Trump S, Hennig BP, Wendisch D, Pott F, et al. COVID-19 severity correlates with airway epithelium–immune cell interactions identified by single-cell analysis. *Nat Biotechnol.* 2020; 38: 970–979. <https://doi.org/10.1038/s41587-020-0602-4> PMID: 32591762
39. Schulte-Schrepping J, Reusch N, Paclik D, Baßler K, Schlickeiser S, Zhang B, et al. Severe COVID-19 Is Marked by a Dysregulated Myeloid Cell Compartment. *Cell.* 2020; 182: 1419. <https://doi.org/10.1016/j.cell.2020.08.001> PMID: 32810438
40. Lee JS, Park S, Jeong HW, Ahn JY, Choi SJ, Lee H, et al. Immunophenotyping of covid-19 and influenza highlights the role of type i interferons in development of severe covid-19. *Sci Immunol.* 2020; 5: 1554. <https://doi.org/10.1126/sciimmunol.abd1554> PMID: 32651212
41. Diaz J V, Baller A, Banerjee A, Bertagnolio S, Bonet M, Bosman A, et al. Clinical management of COVID-19: interim guidance. 2020; WHO/2019-nCoV/clinical/2020.5. <https://www.who.int/publications/i/item/clinical-management-of-covid-19>.
42. Stuart T, Butler A, Hoffman P, Hafemeister C, Papalexi E, Mauck WM, et al. Comprehensive Integration of Single-Cell Data. *Cell.* 2019; 177: 1888–1902.e21. <https://doi.org/10.1016/j.cell.2019.05.031> PMID: 31178118
43. Hafemeister C, Satija R. Normalization and variance stabilization of single-cell RNA-seq data using regularized negative binomial regression. *Genome Biol.* 2019; 20: 296. <https://doi.org/10.1186/s13059-019-1874-1> PMID: 31870423
44. Butler A, Hoffman P, Smibert P, Papalexi E, Satija R. Integrating single-cell transcriptomic data across different conditions, technologies, and species. *Nat Biotechnol.* 2018; 36: 411–420. <https://doi.org/10.1038/nbt.4096> PMID: 29608179
45. McInnes L, Healy J, Saul N, Großberger L. UMAP: Uniform Manifold Approximation and Projection. *J Open Source Softw.* 2018; 3: 861. <https://doi.org/10.21105/joss.00861>
46. Finak G, McDavid A, Yajima M, Deng J, Gersuk V, Shalek AK, et al. MAST: A flexible statistical framework for assessing transcriptional changes and characterizing heterogeneity in single-cell RNA sequencing data. *Genome Biol.* 2015; 16: 278. <https://doi.org/10.1186/s13059-015-0844-5> PMID: 26653891
47. Soneson C, Robinson MD. Bias, robustness and scalability in single-cell differential expression analysis. *Nat Publ Gr.* 2018; 15. <https://doi.org/10.1038/nmeth.4612> PMID: 29481549
48. Zhang X, Lan Y, Xu J, Quan F, Zhao E, Deng C, et al. CellMarker: A manually curated resource of cell markers in human and mouse. *Nucleic Acids Res.* 2019; 47: D721–D728. <https://doi.org/10.1093/nar/gky900> PMID: 30289549
49. Franzén O, Gan LM, Björkegren JLM. PanglaoDB: A web server for exploration of mouse and human single-cell RNA sequencing data. *Database.* 2019; 2019: 46. <https://doi.org/10.1093/database/baz046> PMID: 30951143
50. Monaco G, Lee B, Xu W, Mustafah S, Hwang YY, Carré C, et al. RNA-Seq Signatures Normalized by mRNA Abundance Allow Absolute Deconvolution of Human Immune Cell Types. *Cell Rep.* 2019; 26: 1627–1640.e7. <https://doi.org/10.1016/j.celrep.2019.01.041> PMID: 30726743
51. Wickham H. ggplot2: Elegant Graphics for Data Analysis. Cham: Springer International Publishing; 2016.
52. Cao J, Spielmann M, Qiu X, Huang X, Ibrahim DM, Hill AJ, et al. The single-cell transcriptional landscape of mammalian organogenesis. *Nature.* 2019; 566: 496–502. <https://doi.org/10.1038/s41586-019-0969-x> PMID: 30787437
53. Qiu X, Mao Q, Tang Y, Wang L, Chawla R, Pliner HA, et al. Reversed graph embedding resolves complex single-cell trajectories. *Nat Methods.* 2017; 14: 979–982. <https://doi.org/10.1038/nmeth.4402> PMID: 28825705

54. Trapnell C, Cacchiarelli D, Grimsby J, Pokharel P, Li S, Morse M, et al. The dynamics and regulators of cell fate decisions are revealed by pseudotemporal ordering of single cells. *Nat Biotechnol.* 2014; 32: 381–386. <https://doi.org/10.1038/nbt.2859> PMID: 24658644
55. Alexa A, Rahnenfuhrer J. topGO: Enrichment Analysis for Gene Ontology. *Bioconductor.* 2020;R package.
56. Gu Z, Eils R, Schlesner M. Complex heatmaps reveal patterns and correlations in multidimensional genomic data. *Bioinformatics.* 2016; 32: 2847–2849. <https://doi.org/10.1093/bioinformatics/btw313> PMID: 27207943
57. Gu Z, Gu L, Eils R, Schlesner M, Brors B. Circlize implements and enhances circular visualization in R. *Bioinformatics.* 2014; 30: 2811–2812. <https://doi.org/10.1093/bioinformatics/btu393> PMID: 24930139
58. Kapellos TS, Bonaguro L, Gemünd I, Reusch N, Saglam A, Hinkley ER, et al. Human monocyte subsets and phenotypes in major chronic inflammatory diseases. *Frontiers in Immunology.* *Frontiers Media S. A.*; 2019. p. 2035. <https://doi.org/10.3389/fimmu.2019.02035> PMID: 31543877
59. Chang MY, Kang I, Gale M, Manicone AM, Kinsella MG, Braun KR, et al. Versican is produced by trif- and type I interferon-dependent signaling in macrophages and contributes to fine control of innate immunity in lungs. *Am J Physiol—Lung Cell Mol Physiol.* 2017; 313: L1069–L1086. <https://doi.org/10.1152/ajplung.00353.2017> PMID: 28912382
60. Wang S, Song R, Wang Z, Jing Z, Wang S, Ma J. S100A8/A9 in inflammation. *Frontiers in Immunology.* *Frontiers Media S.A.*; 2018. p. 1298. <https://doi.org/10.3389/fimmu.2018.01298> PMID: 29942307
61. Palomino DC arolin. T, Marti LC avalheir. Chemokines and immunity. *Einstein (São Paulo, Brazil).* Instituto de Ensino e Pesquisa Albert Einstein; 2015. pp. 469–473.
62. Mohr A, Malhotra R, Mayer G, Gorochov G, Miyara M. Human FOXP3+ T regulatory cell heterogeneity. *Clinical and Translational Immunology.* Wiley-Blackwell; 2018. <https://doi.org/10.1002/cti2.1005> PMID: 29484183
63. Okamura T, Fujio K, Shibuya M, Sumitomo S, Shoda H, Sakaguchi S, et al. CD4+CD25-LAG3+ regulatory T cells controlled by the transcription factor Egr-2. *Proc Natl Acad Sci U S A.* 2009; 106: 13974–13979. <https://doi.org/10.1073/pnas.0906872106> PMID: 19666526
64. Weng NP, Araki Y, Subedi K. The molecular basis of the memory T cell response: Differential gene expression and its epigenetic regulation. *Nature Reviews Immunology.* NIH Public Access; 2012. pp. 306–315. <https://doi.org/10.1038/nri3173> PMID: 22421787
65. Sichien D, Scott CL, Martens L, Vanderkerken M, Van Gassen S, Plantinga M, et al. IRF8 Transcription Factor Controls Survival and Function of Terminally Differentiated Conventional and Plasmacytoid Dendritic Cells, Respectively. *Immunity.* 2016; 45: 626–640. <https://doi.org/10.1016/j.immuni.2016.08.013> PMID: 27637148
66. Gavin AL, Huang D, Huber C, Mårtensson A, Tardif V, Skog PD, et al. PLD3 and PLD4 are single-stranded acid exonucleases that regulate endosomal nucleic-acid sensing. *Nat Immunol.* 2018; 19: 942–953. <https://doi.org/10.1038/s41590-018-0179-y> PMID: 30111894
67. Collin M, Bigley V. Human dendritic cell subsets: an update. *Immunology.* Blackwell Publishing Ltd; 2018. pp. 3–20. <https://doi.org/10.1111/imm.12888> PMID: 29313948
68. Camper N, Glasgow AMA, Osbourn M, Quinn DJ, Small DM, McLean DT, et al. A secretory leukocyte protease inhibitor variant with improved activity against lung infection. *Mucosal Immunol.* 2016; 9: 669–676. <https://doi.org/10.1038/mi.2015.90> PMID: 26376365
69. Uhlen M, Fagerberg L, Hallstrom BM, Lindskog C, Oksvold P, Mardinoglu A, et al. Tissue-based map of the human proteome. *Science (80-).* 2015; 347: 1260419–1260419. <https://doi.org/10.1126/science.1260419> PMID: 25613900
70. Zietkiewicz E, Bukowy-Bieryllo Z, Rabiasz A, Daca-Roszak P, Wojda A, Voelkel K, et al. CFAP300: Mutations in slavic patients with primary ciliary dyskinesia and a role in ciliary dynein arms trafficking. *Am J Respir Cell Mol Biol.* 2019; 61: 400–449. <https://doi.org/10.1165/rcmb.2018-0260OC> PMID: 30916986
71. Amodio N, Raimondi L, Juli G, Stamato MA, Caracciolo D, Tagliaferri P, et al. MALAT1: A drug-gable long non-coding RNA for targeted anti-cancer approaches. *Journal of Hematology and Oncology.* BioMed Central Ltd.; 2018. pp. 1–19. <https://doi.org/10.1186/s13045-018-0606-4> PMID: 29739426
72. Bittmann S, Weissenstein A, Villalon G, Moschuring-Alieva E, Luchter E. Simultaneous Treatment of COVID-19 With Serine Protease Inhibitor Camostat and/or Cathepsin L Inhibitor? *J Clin Med Res.* 2020; 12: 320–322. <https://doi.org/10.14740/jocmr4161> PMID: 32489508
73. Zmijewski JW, Pittet JF. Human Leukocyte Antigen-DR Deficiency and Immunosuppression-Related End-Organ Failure in SARS-CoV2 Infection. *Anesthesia and Analgesia.* Lippincott Williams and Wilkins; 2020. pp. 989–992. <https://doi.org/10.1213/ANE.0000000000005140> PMID: 32925313

74. Zheng M, Gao Y, Wang G, Song G, Liu S, Sun D, et al. Functional exhaustion of antiviral lymphocytes in COVID-19 patients. *Cellular and Molecular Immunology*. Springer Nature; 2020. pp. 533–535. <https://doi.org/10.1038/s41423-020-0402-2> PMID: 32203188
75. Mathew D, Giles JR, Baxter AE, Oldridge DA, Greenplate AR, Wu JE, et al. Deep immune profiling of COVID-19 patients reveals distinct immunotypes with therapeutic implications. *Science* (80-). 2020; 369. <https://doi.org/10.1126/science.abc8511> PMID: 32669297
76. yang Yu S, Dong B, Tang L, hua Zhou S. LncRNA MALAT1 sponges miR-133 to promote NLRP3 inflammasome expression in ischemia-reperfusion injured heart. *International Journal of Cardiology*. Elsevier Ireland Ltd; 2018. p. 50. <https://doi.org/10.1016/j.ijcard.2017.10.071> PMID: 29407129
77. Cui H, Banerjee S, Guo S, Xie N, Ge J, Jiang D, et al. Long noncoding RNA Malat1 regulates differential activation of macrophages and response to lung injury. *JCI insight*. 2019; 4. <https://doi.org/10.1172/jci.insight.124522> PMID: 30676324
78. Hirano T, Murakami M. COVID-19: A New Virus, but a Familiar Receptor and Cytokine Release Syndrome. *Immunity*. 2020; 52: 731–733. <https://doi.org/10.1016/j.immuni.2020.04.003> PMID: 32325025
79. Ali S, Hirschfeld AF, Mayer ML, Fortuno ES, Corbett N, Kaplan M, et al. Functional Genetic Variation in NFKBIA and Susceptibility to Childhood Asthma, Bronchiolitis, and Bronchopulmonary Dysplasia. *J Immunol*. 2013; 190: 3949–3958. <https://doi.org/10.4049/jimmunol.1201015> PMID: 23487427
80. Vogler M. BCL2A1: The underdog in the BCL2 family. *Cell Death and Differentiation*. Nature Publishing Group; 2012. pp. 67–74. <https://doi.org/10.1038/cdd.2011.158> PMID: 22075983
81. Du C, Xie H, Zang R, Shen Z, Li H, Chen P, et al. Apoptotic neuron-secreted HN12 inhibits cell apoptosis in Hirschsprung's disease. *Int J Nanomedicine*. 2016; 11: 5871–5881. <https://doi.org/10.2147/IJN.S114838> PMID: 27853370
82. Santofimia-Castaño P, Lan W, Bintz J, Gayet O, Carrier A, Lomberk G, et al. Inactivation of NUPR1 promotes cell death by coupling ER-stress responses with necrosis. *Sci Rep*. 2018; 8. <https://doi.org/10.1038/s41598-018-35020-3> PMID: 30451898
83. Laha S, Saha C, Dutta S, Basu M, Chatterjee R, Ghosh S, et al. In silico analysis of altered expression of long non-coding RNA in SARS-CoV-2 infected cells and their possible regulation by STAT1, STAT3 and interferon regulatory factors. *Heliyon*. 2021; 7: e06395. <https://doi.org/10.1016/j.heliyon.2021.e06395> PMID: 33688586
84. Plowman T, Lagos D. Non-Coding RNAs in COVID-19: Emerging Insights and Current Questions. *Non-Coding RNA*. 2021; 7: 54. <https://doi.org/10.3390/ncrna7030054> PMID: 34564316
85. Rodrigues AC, Adamoski D, Genelhould G, Zhen F, Yamaguto GE, Araujo-Souza PS, et al. NEAT1 and MALAT1 are highly expressed in saliva and nasopharyngeal swab samples of COVID-19 patients. *Mol Oral Microbiol*. 2021 [cited 11 Oct 2021]. <https://doi.org/10.1111/omi.12351> PMID: 34463043
86. Yang Q, Lin F, Wang Y, Zeng M, Luo M. Long Noncoding RNAs as Emerging Regulators of COVID-19. *Frontiers in Immunology*. Frontiers Media S.A.; 2021. p. 3076. <https://doi.org/10.3389/fimmu.2021.700184> PMID: 34408749